8-2017

# Brain Microvascular Injury and White Matter Disease Provoked by Diabetes-Associated Hyperamylinemia

Han Ly
*University of Kentucky*

Nirmal Verma
*University of Kentucky*, nirmal.verma@uky.edu

Fengen Wu
*University of Kentucky*

Miao Liu
*University of Kentucky*, m.liu@uky.edu

Kathryn E. Saatman
*University of Kentucky*, k.saatman@uky.edu

# Brain Microvascular Injury and White Matter Disease Provoked by Diabetes-Associated Hyperamylinemia

Digital Object Identifier (DOI)
https://doi.org/10.1002/ana.24992

## Notes/Citation Information

Published in *Annals of Neurology*, v. 82, issue 2.



## Authors

Han Ly, Nirmal Verma, Fengen Wu, Miao Liu, Kathryn E. Saatman, Peter T. Nelson, John T. Slevin, Larry B. Goldstein, Geert Jan Biessels, and Florin Despa

HHS Public Access

Author manuscript

*Ann Neurol*. Author manuscript; available in PMC 2018 August 01.

Published in final edited form as:

*Ann Neurol*. 2017 August ; 82(2): 208–222. doi:10.1002/ana.24992.

# Brain microvascular injury and white matter disease provoked by diabetes-associated hyperamylinemia

**Han Ly, BS**[1], **Nirmal Verma, PhD**[1], **Fengen Wu**[1], **Miao Liu, PhD**[1], **Kathryn E. Saatman, PhD**[2,3], **Peter T. Nelson, MD, PhD**[4], **John T. Slevin, MD**[5,6], **Larry B. Goldstein, MD**[6], **Geert Jan Biessels, MD, PhD**[7], and **Florin Despa, PhD**[1,6]

[1]Department of Pharmacology and Nutritional Sciences, University of Kentucky, Lexington, KY, USA [2]Spinal Cord and Brain Injury Research Center, University of Kentucky, Lexington, KY, USA [3]Department of Physiology, University of Kentucky, Lexington, KY, USA [4]Sanders-Brown Center on Aging, University of Kentucky, Lexington, KY, USA [5]Veterans Administration Medical Center, Lexington, KY, USA [6]Department of Neurology, University of Kentucky, Lexington, KY, USA [7]Department of Neurology, University Medical Center Utrecht, Utrecht, The Netherlands

## Abstract

**Objectives—**The brain blood vessels of patients with type-2 diabetes and dementia have deposition of amylin, an amyloidogenic hormone co-secreted with insulin. It is not known whether vascular amylin deposition is a consequence or a trigger of vascular injury. We tested the hypothesis that the vascular amylin deposits cause endothelial dysfunction and microvascular injury and are modulated by the amylin transport in the brain via plasma apolipoproteins.

**Methods—**Rats overexpressing amyloidogenic (human) amylin in the pancreas (HIP rats) and amylin knockout (AKO) rats intravenously infused with aggregated amylin were used for *in vivo* phenotyping. We also carried out biochemical analyses of human brain tissues and studied the effects of the aggregated amylin on endothelial cells, *ex vivo*.

**Results—**Amylin deposition in brain blood vessels is associated with vessel wall disruption and abnormal surrounding neuropil in patients with type-2 diabetes and dementia, in HIP rats, and in AKO rats infused with aggregated amylin. HIP rats have brain microhemorrhages, white matter injury and neurologic deficits. Vascular amylin deposition provokes loss of endothelial cell coverage and tight junctions. Intravenous infusion in AKO rats of human amylin, or combined human amylin and apolipoprotein E4, showed that amylin binds to plasma apolipoproteins. The intravenous infusion of apolipoprotein E4 exacerbated the brain accumulation of aggregated amylin and vascular pathology in HIP rats.

Correspondence: Florin Despa, Department of Pharmacology and Nutritional Sciences, College of Medicine, University of Kentucky, Wethington Building, Room 459, 900 S. Limestone, Lexington, Kentucky, 40536, USA. Phone: 859-218-0291. Fax: 859-257-3646. f.despa@uky.edu.

**Author contributions**

Conception and design of the study: F.D. Acquisition and analysis of data: H.L., N.V., F.W., M.L., P.T.N., K.E.S. Drafting and revision of the manuscript: F.D., H.L., L.B.G., G.J.B., J.T.S., P.T.N. and K.E.S.

**Potential conflicts of interest:** Nothing to report.

**Interpretation—**These data identify vascular amylin deposition as a trigger of brain endothelial dysfunction that is modulated by plasma apolipoproteins and represents a potential therapeutic target in diabetes-associated dementia and stroke.

## Introduction

Microvascular-related brain injury is associated with focal neurologic deficits and dementia[1–5]. The distal territories of small penetrating vessels (arterioles and capillaries) supplying brain white matter are particularly vulnerable to vascular pathologies (also known as cerebral small vessel disease). High blood pressure, atherosclerosis and inflammation are among the major causes of brain white matter disease of vascular origin[1–5]. Recent investigations[6–8] have revealed that the brain microvasculature of patients with dementia contains large deposits of amylin, a ~4 kDa peptide co-synthesized with insulin by pancreatic β-cells[9]. Vascular deposition of amylin is particularly abundant in the brains of patients with dementia and type-2 diabetes[6,7]. The peptide amylin (or islet amyloid polypeptide) normally crosses the blood brain barrier[10] and binds to neurons in the feeding centers[11,12], where it is believed to induce an anorexic effect[13,14]. In patients with type-2 diabetes, amylin forms amyloid in the pancreatic islets that triggers β-cell apoptosis[9,15,16]. Deposits of aggregated amylin are also identified in failing hearts[17,18] and kidneys[19] of individuals with type-2 diabetes or obesity. Of note, apolipoprotein E4 (APOE4), which is strongly associated with β amyloid (Aβ) pathology[20,21], modulates amylin aggregation[22] and amylin amyloid formation[23,24].

Amylin from species that do not develop type-2 diabetes (i.e. mice and rats) is non-amyloidogenic due to proline substitutions at the 25, 28, and 29 sites[25]. Pharmacological induction of insulin resistance in transgenic mice expressing the amyloidogenic amylin variant (i.e., human amylin) caused intra- and extracellular amylin amyloid deposition, β-cell apoptosis and overt hyperglycemia[26]. Similar pathologic changes occur in rodents *overexpressing* human[27], but not murine amylin[16]. We previously reported that rats overexpressing human amylin in the pancreas accumulate aggregated amylin in the brain[28], which correlates with the development of neuroinflammation[28,29], reduced synthesis (by >50%) of catecholamine precursors (phenylalanine and tyrosine)[30] and neurologic deficits[28]. Furthermore, a recent study demonstrated that transgenic mice overexpressing human amylin in pancreatic islets and a mutant form of the amyloid precursor protein (APP) in neurons have exacerbated Aβ pathology compared to transgenic mice expressing only one or the other protein[31].

Distinct from other diabetic complications, glucose dysregulation does not appear to be the primary determinant of progressive brain injury in patients with diabetes[32–37]. The pathophysiology underlying slowly progressive functional and structural brain changes in the setting of type-2 diabetes is largely unknown[32–37]. Given the toxicity of aggregated amylin[9,15–19], we hypothesized that the complex pathophysiology[32–37] underlying slowly progressive functional and structural brain changes in patients with type-2 diabetes involves accumulation of aggregated amylin in the brain blood vessels. Here, we tested the hypothesis that aggregated amylin circulates through the blood, deposits in brain blood vessels (possibly via the interaction with plasma apolipoproteins) and provokes brain

microvascular injury by degrading endothelial cell coverage and tight junctions. To test this hypothesis, we performed *in vivo* phenotyping of rats expressing amyloidogenic (human) amylin in the pancreas (HIP rats[27]) and generated amylin knockout (AKO) rats that were intravenously infused with aggregated human amylin. We also carried out biochemical analyses of brain tissues from humans and studied the effects of the aggregated amylin on endothelial cells, *ex vivo*. Our findings may contribute to the understanding of the complex molecular mechanisms underlying the diabetes-associated stroke and dementia[32–37].

## Methods

This investigation conforms to the Guide for the Care and Use of Laboratory Animals published by the US National Institutes of Health (NIH Publication No. 85-23, revised 1996) and was approved by the Institutional Animal Care and Use Committees at University of Kentucky.

Paraffin embedded brain tissues were provided by the Alzheimer's Disease Center biobank at the University of Kentucky. The protocol was approved by the Institutional Review Board.

For immunohistochemistry, formalin fixed dorsolateral frontal cortex (Brodmann area 9) tissue was used from three autopsied individuals >80 years of age at death, with type-2 diabetes and dementia and three age-matched cognitively normal individuals without type-2 diabetes (Supplementary Table 1). The absence/presence of diabetes was determined during life (at longitudinal clinical visits) by patient or caregiver self-report and the use of diabetic medications[38]. The assessment of clinical dementia and the neuropathologic features - neuritic amyloid plaques (Consortium to Establish a Registry for Alzheimer's Disease; CERAD), Braak NFT stage and cerebral amyloid angiopathy (CAA) severity - were scored as previously described[39–43]. Neuropathological information, *APOE* genotype, age and sex of each individual included in the present study are summarized with specific findings related to the vascular amylin pathology.

### Experimental animals

HIP rats (n = 79; breeding pairs provided by Charles River Laboratory) were used in behavior testing and physiological analyses. HIP rats are Sprague-Dawley rats that overexpress (3-fold) human amylin in the pancreatic β-cells[27]. Wild-type (WT) littermate rats (n = 49) were used as non-diabetic controls.

AKO rats were used to identify a possible interaction of amylin with plasma apolipoproteins (*APOE*) and to test whether intravenous infusion of aggregated human amylin injures the brain microvessels independently of glucotoxicity. AKO rats (rather than WT rats) were used in amylin-injection experiments to eliminate the confound that rodent amylin and human amylin form mixed oligomers[44]. AKO rats were generated in collaboration with *Transposagen Biopharmaceuticals* (Lexington, KY). The rat amylin gene was targeted at two sites by producing double strand breaks in the genome using the CRISPR/CAS9 system[45]. The CRISPR gRNAs and Cas9 mRNA were microinjected into the pronucleus of fertilized Sprague-Dawley rat embryos by standard techniques and the embryos were reimplanted to produce the genetically modified offspring. Amylin gene knock-out was confirmed by

genotyping using the following primers for DNA amplification: Forward: 3′-AGAGCTAAGCAAGTTGAGGGAT-5′, and Reverse: ACCACTAGTTCACATTCACAGAGG. AKO rat pancreas was tested for amylin immunoreactivity signal by Western blot.

## Behavior testing

**Inclined plane—**Rats were placed on the flat plane in the horizontal position with head either facing up or down to the side to be raised. Starting at 30°, the angle was increased at 2°/second. The angle at which the animal starts to free-fall was recorded. Each rats received 3 trials per head facing direction. Rats were allowed to rest 1 minute between trials. Results were averaged for 6 trials.

**Cylinder test/Forelimb use test—**To evaluate forelimb deficits, the animal was placed in a transparent cylinder for 5 minutes, and the activity was videorecorded. The time that forepaws contacted with the cylinder wall during vertical rearing up was calculated using slow-motion playback software (Kinovea).

**Morris Water Maze—**Visuospatial learning and memory retention was tested in a 1.5 m diameter Morris Water Maze[46]. HIP and WT littermate rats with no motor impairments were given 10 learning trials per day for two consecutive days using random starting locations (N, E, S, W). Animals were allowed to stand on the platform for 30 s after the first trial and 15 s after each additional trial. If the animals failed to locate the platform, they were picked up and put on the platform for 15 s. To assess reference memory, a probe trial was given 24 hours after the second acquisition day. The probe trial was scored on latency to cross the platform. Trials were recorded by EthoVision XT software (Noldus, VA).

## Magnetic resonance imaging

MRI data were acquired using a horizontal 7T nuclear magnetic resonance scanner (ClinScan, Bruker BioSpin MRI, Ettlingen, Germany) and a 38-mm rat brain coil. Rats were first anesthetized with isoflurane (4.0% for induction, 1.2% for maintenance) and air mixture. Heart rate (90 to 130 b.p.m.), respiration rate, and rectal temperature (37±0.5°C) were continuously monitored. Heart rate and blood oxygen saturation level were maintained within normal physiological ranges. Coronal $T_2$-weighted MR images were obtained using the following variables: repetition time (TR), 3000 ms; echo time (TE), 24 ms; field of view (FOV), 2.5 × 2.5 $cm^2$; acquisition matrix 128 × 128; thickness, 1mm, 7 slices. Ventricular volume was measured from the frontal horn of lateral ventricle to the foramen of Luschka by combining hyper-intense ventricular area using ImageJ over all slices and multiplying by section thickness[47]. Similarly, total brain volume was measured by multiplying combined brain area over all slices to section thickness. Parenchymal volume was calculated by subtracting ventricular volume from total brain volume.

## Isolation of rat brain capillaries

Freshly isolated brain was homogenized in capillary PBS (cPBS) (137 mM NaCl, 2.7 mM KCl, 8.1 mM $Na_2HPO_4$, 1.47 mM $KH_2PO_4$, 1.05 mM $MgCl_2$, 0.9 mM $CaCl_2$, 5 mM glucose, 0.9 mM sodium pyruvate). To separate blood vessels from brain parenchyma, the

brain homogenate was centrifuged in 30% Ficoll PM 400 solution (F-4375, Sigma, MO) at 5000 x*g* for 20 minutes, 4°C. The capillaries were then isolated by the glass-bead column filtration method. In the first step, the pellet resulting from the centrifugation was re-suspended with 1% BSA in cPBS and passed through a 300 μm strainer. Then, the filtered pellet suspension was added into the glass bead column. Two hundred ml 1% BSA was passed through the column. Capillaries were retrieved from the beads by agitation in 1% BSA and filtering through a strainer, followed by centrifugation at 500 x*g* for 5 minutes, 4°C. Capillaries were washed twice with cPBS before the experiment. For quality control, capillaries were stained with Texas red dye and were examined under confocal microscope.

## Cerebral blood flow measurement

Fluorescent microspheres (15 μm diameter; F8839, Thermo Fisher, MA) were vortexed for 30 s in heparinized saline ($10^6$/mL fluorescent microspheres). Anesthetized HIP and WT rats were injected with a 200 μl volume containing microspheres and heparinized saline through the jugular line, twice (15 mins apart). Animals were sacrificed and the brains collected for tissue digestion, capillary isolation (as described above) and microsphere recovery by filtration followed by fluorescence measurements.

Equal weights of brain capillaries and remaining parenchymal tissue from WT and HIP rats were individually digested in 4M KOH and 2% tween 80 (Sigma Aldrich, MO). The tissue was completely digested within 24 hours. The digested tissue was then filtered through 10μm pore polycarbonate filters (Millipore, CA). The vial and filtering syringe were washed twice with 2% tween, and wash was filtered to recover residual microspheres. The filter and filtered material from each tissue were placed in 1.25 ml of Cellosolve acetate (Sigma Aldrich, MO) in tubes. After ≥4 and up to 24 hours, 100μl samples from each tube were placed in a 96 well microplate and the florescence of each was determined by florescent spectrophotometer.

## Histology

HIP, WT and AKO rat brains were analyzed by staining with Prussian blue and Luxol fast blue (LFB). For Prussian blue staining, sections were microwaved in solution containing 5% HCl and 5% potassium ferrocyanide (14459-95-1, Acros, Geel, Belgium). Nuclei were stained with neutral red (N7005, Sigma, MO). For Luxol fast blue staining, sections were treated with luxol fast blue (AC212170250, Acros, Geel, Belgium) solution O/N at 56°C, followed by 95% ethanol and $dH_2O$ rinse. Slides were differentiated in lithium carbonate solution then 70% ethanol, followed by H&E staining (BP2424-25, E511-100, Fisher, PA). Images were obtained on the Nikon Eclipse 55i upright microscope (Nikon).

## Immunohistochemistry

We used brain tissues from humans, HIP, WT and AKO rats. Tissues were processed as previously described[6,29]. Antibodies against amylin (1:200, T-4157, Bachem-Peninsula Laboratories, CA), glial fibrillary acidic protein (GFAP; 1:600, MAB360, Millipore, MA) or myelin basic protein (MBP; 1:5,000, AMAB91064, clone CL2829, Sigma, MO) were the primary antibodies. Anti-mouse or anti-rabbit IgG (1:50, A3562, A3687, Sigma, MO) were

secondary antibodies. The specificity of the amylin antibody in both human and rat brain tissues was established in previous studies[6,7,29].

### Demyelination scoring

Demyelination of the white matter (MBP and LFB staining) was scored by a blinded observer. Ordinal pathologic scoring was used, ranging from normal to severe demyelination (0–3)[48].

### Immunofluorescence

We used brain tissues from humans, HIP, WT and AKO rats, and isolated brain capillaries from HIP, WT and AKO rats. Brain tissue was processed as previously[29] described. Brain capillaries were isolated (as described above) and then plated on laminin (23017-015, Gibco, MA) coated chambered coverglass for 1-hour, to allow time to attach.

Antibodies against human amylin (1:200, SC-377530, Santa Cruz, TX), collagen IV (1:500, SAB4200500, Sigma, MO), caveolin1 (1:1,000, sc-894, Santa Cruz, TX) and APOE (1:200, ab183597, Abcam, MA) were the primary antibodies. Alexa Fluor 488 conjugated anti-mouse IgG (A11029, Invitrogen, MA) and Alexa Fluor 568 conjugated anti-rabbit IgG (A11036, Invitrogen, MA) were the secondary antibodies.

### Immunoprecipitation

HIP rat plasma was investigated in these experiments. Protein concentration was determined by BCA protein assay prior to immunoprecipitation. APOE was precipitated from 700 μg plasma protein. Samples were incubated at 4°C O/N with 5 μg anti-APOE antibody (ab183597, Abcam, MA) or anti-APOA-1 antibody (H00000335-D01P, Abnova). Antibody-antigen complex was precipitated out by protein A/G agarose (20421, Thermo Scientific), rotated for 3 hours at 4°C. Immunoprecipitates were collected by centrifugation followed by washing three times with buffer (5 mM EGTA, 50 mM Tris, 1% Triton X-100, phosphatase and protease inhibitors 1:100 ratio, pH 7.5). Proteins were eluted two times with elution buffer (0.2 M Glycine, 80 mM HCl, pH 2) and incubated on ice for 5 min with the supernatant collected by centrifugation. Centrifugation speed was 1000 x*g* for 1 min at 4°C. Samples were re-suspended in loading buffer and subjected to western blotting.

### Western blot analysis

Western blot analysis was performed on isolated brain capillaries from rats and plasma and whole blood lysates from rats and humans. Plasma and whole blood were processed as described previously[6,18]. Capillaries were isolated as described above and then lysed in buffer containing 1% NP-40, 150mM NaCl, 10mM Tris-HCl, 2mM EGTA, 50mM NaF, 1% phosphatase and 1% protease inhibitors. The lysate was centrifuged at 17,000 xg for 30 minutes. The supernatant was used for Western blotting. Primary antibodies against amylin (1:2,000, T-4157, Bachem-Peninsula Laboratories, CA), occludin (1:300, 71-1500, Invitrogen, MA), claudin-5 (1:1,000, 35-2500, Invitrogen, MA), ZO-1 (1:300, 61-7300, Invitrogen, MA), collagen IV (1:1,000, ab6586, Abcam, MA), caveolin1 (1:1,000, sc-894, Santa Cruz) or β-actin (1:10,000, PIMA515739, Fisher, PA) were used in these analyses. Equal loading in Western blot experiments was verified by re-probing with a monoclonal

anti-β actin antibody (raised in mouse, clone BA3R, Thermo Scientific; 1:2000). Protein levels were compared by densitometric analysis using ImageJ software.

### Real-Time Quantitative Reverse Transcription PCR

Expression levels of caveolin-1 and collagen IV in rat brain capillaries were measured using a protocol described previously[29]. Caveolin-1 primers (forward: 5′-CTTAAATCACAGCCCAGGGAAAC-3′ and reverse: 5′-GCGTCGTACACTTGCTTCTC-3′) and collagen IV primers (forward: 5′-AAATGGCGCTCCTGATCCAA-3′ and reverse: 5′-TTCTTGTGGAGTTCTCGCCC-3′) were used in these experiments. Actin primers (forward: 5′-CTGGCTCCTAGCACCATGAA-3′ and reverse: 5′-AAAACGCAGCTCAGTAACAGTC-3′) were used as internal controls.

### Cell culture and flow cytometry analysis

Prior to plating, culture flasks were coated with cell attachment factor solution (123-100, Sigma, MO). Brain microvascular endothelial cells from WT adult Sprague Dawley rats (RA-6023, Cell Biologics, Chicago, IL) were plated for 24 hours and used for experiment when they reached 70%–90% confluency. Cells were incubated with 50 μM human amylin (AS-60804, AnaSpec, CA) for 2 hours at $37^0$C. Cells were dissociated with trypsin and washed with cold PBS before being stained with PI and Annexin V, according to manufacture protocol (V13241, Life Technologies, MA). Apoptotic cells and necrotic cells were detected with analytical flow cytometer (Becton-Dickinson LSRII).

### Statistical analysis

Parametric comparison of two groups was done using two-tailed unpaired t-test. Non-parametric comparison of two groups was done using Mann–Whitney unpaired t-test. Two-ways analysis of variance with repeated measures followed by Bonferroni *post-hoc* tests were used to analyze the Morris water maze data. Data are presented as means ± s.e.m. Difference between groups was considered significant when $P < 0.05$. All analyses were performed using GraphPad Prism 5.0 software.

## Results

### Impaired neurological functioning upon inducing amylin dyshomeostasis in rats

Both male and female HIP rats had increased plasma levels of amylin (Fig 1A) and developed overt hyperglycemia (>200 mg/dl; non-fasted; Fig 1B). Western blot analysis of amylin in plasma samples (Fig 1A) showed multiple molecular weight bands (higher amylin immunoreactive signal is seen in HIP rats compared to WT rats). The higher molecular weight bands could correspond to circulating amylin aggregates, as suggested by previously published data[18,28,49], or amylin binding to plasma components (including plasma APOE; see below).

In contrast to WT littermate rats that had normal behavior, HIP rats had gait abnormalities and impaired balance (Supplementary movies) spontaneous forelimb use (Fig 1C), hind limb clasping (Fig 1D) and altered balance on a stationary inclined plane (Fig 1E). HIP rats and

WT controls had similar swim speeds (Fig 1F); however, latency to platform over the twenty learning trials was longer for HIP rats compared to WT littermates (Fig 1G; two-way ANOVA; P=0.03) indicating that HIP rats had impaired learning. Reference memory, defined as the latency to cross the platform at 24 hours after the second acquisition day (probe trial; Fig 1H), was similar for HIP and WT rats indicating no significant memory deficits associated with amylin dyshomeostasis once the task had been learned. Compared to males, female HIP rats developed hyperglycemia and neurologic deficits (Fig 1B and Supplementary movies) later in life (i.e., ~12 months vs. ~18 months of age). Balance and gait abnormalities were milder in females compared to male HIP rats.

## Brain white matter injury in HIP rats

Based on *in vivo* magnetic resonance imaging (MRI; $T_2$-weighted sequences), the brains of HIP rats had structural abnormalities (Fig 2A), which were not present in control WT littermates. Compared to controls, brains of diabetic male HIP rats showed areas of high $T_2$ signal in the lateral hippocampus and around the temporal horns of the lateral ventricles (Fig 2A; arrows) and expansion of the ventricles (Fig 2B). Expansion of the ventricles and the high $T_2$ signal in the surrounding tissue (Fig 2B) may reflect defects in the resorption of cerebrospinal fluid or/and subcortical atrophy. Because the current MRI protocol did only include coronal $T_2$ images, we cannot formally distinguish between these possibilities.

The volume of brain parenchyma was smaller in diabetic animals compared to controls (Fig 2C). Injured ependyma (arrow head; Fig 2D) and amylin deposition in choroid plexus (Fig 2E) was found in HIP rats with considerably enlarged ventricles.

The brains of rats with falls and impaired balance often revealed intracerebral hemorrhages (arrow; Fig 2F), which were not found in control WT littermates.

We used the fluorescent microsphere technique to assess the brain perfusion status in diabetic HIP rats relative to controls. The retrieval of fluorescent microspheres was lower in brain capillaries (but not parenchymal tissue) of HIP rats compared to controls (Fig 2G) suggesting brain hypoperfusion in HIP rats.

Immunohistochemical analysis of brain paraffin sections (corpus callosum, lateral ventricle area, thalamus and hypothalamus) from diabetic rats showed parenchymal rarefaction. HIP rat brains had a loss of MBP immunoreactivity compared to brains from control animals (Fig 3A). LFB stain of the white matter (Fig 3B) showed the same degree of myelin loss in the brains of diabetic rats compared to controls. Vacuoles were found through the entire white matter in HIP rats compared to controls.

## Cerebral microhemorrhages and perivascular astrocyte recruitment in HIP rats

Histologic analysis of brain tissues from HIP rats showed microhemorrhages (Fig 4A; staining with Prussian blue dye). Serial staining of the periventricular region with the amylin antibody (Fig 4B) showed amylin deposits in microvessels (red arrows) and perivascular areas (inset; brown deposits). Vascular amylin deposition coincided with white matter vacuolation (arrow head). At higher magnification, the same brain area stained with hematoxylin and eosin (H&E) showed loss of cellular details and erythrocytes around a

blood vessel (Fig 4C). Amylin was present within the vessel wall (Fig 4D) and was associated with enlarged Virchow-Robin spaces. In contrast, tissue sections from similar levels of the brain from a WT animal had no vascular or tissue abnormalities. Staining for GFAP revealed robust recruitment of astrocytes in areas of vascular tissue damage (Fig 4E), whereas sections taken at a similar level of the hypothalamus from a control animal lacked obvious abnormalities, including no astrocytosis near intact microvessels. Amylin deposition was also found in association with infarction cores (as in Fig 4F) and disrupted vessel walls (Fig 4G,H). Amylin deposition was also present in hippocampal capillaries of HIP rats (Fig 4I).

## Cerebral microhemorrhages and perivascular astrocyte recruitment following intravenous infusion of aggregated amylin in AKO rats

HIP rats had elevated circulating levels of aggregated amylin (Fig 1A). To test whether circulating aggregated amylin injures the endothelium independently of glucotoxicity, we generated rats with deleted amylin gene (AKO rats; Fig 5A–D). AKO rats were intravenously infused with aggregated human amylin (2 μg/g body weight, q.d., 7 days; approximately three order of magnitude higher than the physiological level of amylin in HIP rats). Western blot analysis of blood lysates from amylin-infused AKO rats, HIP rats and human with type-2 diabetes showed similar distributions of amylin-positive molecular complexes (Fig 5E). Infusion of aggregated amylin provoked accumulation of amylin in the brain microvessels (Fig 5F), astrocyte recruitment in areas of vascular injury (Fig 5G) and brain microhemorrhages (Fig 5H); however, the white matter in amylin-injected animals was intact as assessed by *in vivo* MRI (Fig 5I).

## Vascular amylin deposition is modulated by the amylin-*APOE* interaction

To test for a possible interaction of amylin with APOE *in vivo*, AKO rats (which express rat *APOE*, but lack amylin) were intravenously infused with combined aggregated human amylin (2 μg/g body weight) and *APOE*4 (1.2 μg/g body weight), or only aggregated human amylin for seven days (q.d.). Western blot analysis of plasma samples from rats in the two groups showed greater amylin binding to APOE4 compared to the endogenous rat *APOE* (Fig 6A), consistent with previous *ex vivo* data demonstrating that *APOE*4 modulates amylin aggregation[22]. To further test the interaction of amylin with plasma *APOE*, plasma samples from HIP rats were enriched in *APOE* by immunoprecipitation and were analyzed by Western blot with an anti-amylin antibody. Fig 6B depicts amylin that formed molecular complexes with plasma *APOE* in HIP rats. Not surprisingly, amylin bound to other plasma apolipoproteins as indicated by the immunoreactivity signal of amylin in *APOA*-I enriched by immunoprecipitation (Fig 6B)

Because amylin appears to bind to *APOE*4 (Fig 6A) *in vivo*, we hypothesized that infusion of APOE4 would exacerbate systemic amylin dyshomeostasis and cerebral vascular injury in HIP rats. To test this hypothesis, HIP rats were intravenously infused with APOE4 (1.2 μg/g body weight, q.d., for 7 days). The infusion of *APOE*4 enhanced amylin accumulation in the brains of HIP rats (Fig 6C,D). Fig 6D depicts leakage of amylin from a brain microvessel of a HIP rat that was infused with *APOE*4. No obvious extravasation of *APOE*4 was present in the *APOE*4-infused HIP rats.

## Shared feature of amylin vasculopathy in brains of HIP rats, human amylin-infused AKO rats and human with dementia and type-2 diabetes

Immunohistochemical analysis with an amylin antibody of brain tissues from patients with type-2 diabetes and dementia (T2D-De) showed vascular changes associated with amylin deposition. Fig 7A and B display sections from the brain of a 93 year old man (*APOE* 4/4 carrier with type-2 diabetes and CERAD definite AD, Braak stage V and CAA severity 2). The vascular histopathology includes amylin deposits in the smooth muscle layer of arterioles (Fig 7A) and distortion of the amylin-positive vascular wall contours in capillaries (Fig 7B). Fig 7C shows a brain section from a 92 years old woman with type-2 diabetes and unknown *APOE* genotype (CERAD definite AD, Braak stage V and CAA severity 3). Amylin deposition was found in association with disruption of the vessel wall (Fig 7C). Fig 7D is from the brain of another man (91 years old, *APOE* 3,4 carrier, CERAD definite AD, Braak stage V, but no CAA). Amylin immunoreactivity signal was detected in an area corresponding to a chronic infarct. In the brain that is displayed in Fig 7A, amylin is co-localized with perivascular reactive astrocyte recruitment in disrupted blood vessel walls (Fig 7E). Reactive astrocytosis was lower around blood vessels of aged control individuals, with the caveat of the limited sample size. These pathologic changes were not present in the brain blood vessels of healthy aged individuals. Fig 7F provides a representative section from the 3 brains investigated in this study. Immunoconfocal microscopy analysis of amylin and collagen IV, a component of the basement membrane structure of the blood vessels, in the brain tissue from the 91 years old patient described above showed amylin deposition in an arteriole (arrow; Fig 7G) and a presumed capillary profile (head arrow; Fig 7G). Brain microvessels of HIP rats (Fig 7H) and AKO rats that were intravenously infused with aggregated human amylin (Fig 7I) had similar amylin deposits as in dementia patients who also had type-2 diabetes. In contrast, brain sections from a WT rat showed no amylin staining in brain blood vessels (Fig 7J).

## Vascular amylin deposition injures endothelial cells and degrades tight junction components

To assess the impact of aggregated amylin on the endothelium, cerebral capillaries were isolated from HIP and WT rat brains and stained for amylin and caveolin-1, a protein that is abundant in endothelial cells. Areas of amylin deposition (green) showed weak immunoreactive caveolin signal (red; Fig 8A) suggesting the loss of endothelial cells. Consistent with immunoconfocal data, Western blot analysis demonstrated depletion of caveolin and collagen in brain capillary lysates from HIP rats compared to WT littermates (Fig 8B). There was similar depletion of collagen and caveolin-1 in human amylin-infused AKO rats (Fig 8B). The transcript levels for caveolin-1 and collagen IV were unchanged (Fig 8C) suggesting that the loss of capillary stability was associated with degradation of basement membrane structure and endothelium.

A flow cytometry analysis of cultured brain microvascular endothelial cells from rats was performed to test the viability of endothelial cells after exposure to aggregated human amylin. The interaction of aggregated human amylin with endothelial cells resulted in a significant increase of both early apoptotic (AnV+/PI−) and end-stage apoptotic (AnV+/PI+) populations, and a reduction of the live cell population (AnV−/PI−; Fig 8D).

The tight junction components, claudin, occludin and ZO adapter proteins were degraded in cerebral capillaries from HIP rats (Fig 8E). There was some reduction in tight junction components in amylin-infused AKO rats (Fig 8E). Thus, microhemorrhages and amylin vasculopathy in HIP rat brains were associated with endothelial damage.

## Discussion

Our data suggest that the amyloidogenicity of the human amylin peptide, amylin hypersecretion and plasma APOE are important mediators of amylin deposition in the cerebral microvasculature. Vascular amylin deposition was associated with endothelial cell damage and degradation of tight junctions that could explain the associated microhemorrhages and recruitment of perivascular astrocytes that occurred in HIP rats and in AKO rats infused with aggregated human amylin. Accumulated injury to cerebral small vessels can contribute to hypoperfusion leading to injury of brain parenchyma, loss of brain volume, and neurologic deficits (as seen in HIP rats; Fig 8F – proposed mechanism). Our findings are consistent with previous reports that implicated amylin dyshomeostasis as a contributor to the development of type-2 diabetes[9,15,16,25–27] and cardiovascular disease[17–19]. The most important finding of this study is the demonstration of amylin-provoked microhemorrhages in HIP rats and AKO rats infused with aggregated human amylin. This provides direct evidence that diabetes-associated amylin dyshomeostasis provokes a microangiopathy. This is a noteworthy finding because amylin deposits are present in the brain microvessels of patients with type-2 diabetes and dementia. Cerebral microhemorrhages occur frequently in patients with both ischemic and hemorrhagic stroke[50] and in individuals with cerebral amyloid angiopathy (CAA)[4]. Different from CAA, brain microvessels in AKO rats infused with aggregated human amylin showed concentric amylin deposition indicating that circulating aggregated amylin results in luminal amylin deposition. Thus, amylin-mediated narrowing of brain microvessels is a likely contributor to brain hypoperfusion and parenchymal loss leading to impaired neurological functioning in diabetic HIP rats. Cerebral microvascular injury that occurs in patients with type-2 diabetes is suggested to result from nonenzymatic glycation of proteins and subsequent production of toxic derivatives that induce endothelial cell oxidative damage[32,33]. The induction of cerebral microhemorrhages and surrounding neuropil injury occurred in amylin-infused AKO rats in the absence of hyperglycemia, which suggests that circulating aggregated amylin is a pathologic substrate for endothelial dysfunction in the setting of diabetes. Further study is required to establish a causal link between the level of circulating amylin and the effect of the resulting microvascular injury on brain parenchyma and functional outcomes in humans.

The cellular and molecular mechanisms that underlie the impact of cerebral microvascular injury on neural circuit function are complex and incompletely understood. This limitation stems in part from a paucity of experimental models[51,52]. In HIP rats, neurological deficits are associated with white matter injury caused by vascular amylin deposition. The present results indicate that expressing human amylin in species that do not develop type-2 diabetes (i.e. mice and rats) can provide a means to better understand the complex vascular factors affecting white matter integrity in patients with diabetes and dementia.

APOE is a plasma protein that serves as a ligand for low density lipoprotein receptors, participates in the transport of cholesterol and other lipids among various cells of the body[53] and is present in amylin amyloid-containing pancreatic tissue from humans[23,24]. The infusion of APOE4 exacerbated amylin-mediated capillary injury and brain amylin accumulation in HIP rats. The result suggests an interaction between amylin and plasma APOE as a potential mechanism underlying brain amylin pathology. Because APOE4 may modulate amylin aggregation[22], we speculate that elevated levels of plasma APOE4 could trigger the formation of toxic amylin aggregates in the blood. Additional studies are needed to elucidate the potential role of APOE alleles in promoting vascular amylin deposition.

Amylin plays a complex role in modulating the peripheral energy balance[11–14]. We demonstrated that systemic amylin dyshomeostasis contributes to the microvascular injury in the setting of diabetes. Thus, amylin dyshomeostasis may be a therapeutic target in diabetes-associated stroke and dementia.

## Supplementary Material

Refer to Web version on PubMed Central for supplementary material.

## Acknowledgments

This research was supported by National Institutes of Health (R01AG053999, R01HL118474 and pilot fund from Sanders-Brown Center on Aging AG028383-09 to FD), Alzheimer's Association (VMF-15-363458 to FD) and American Stroke Association (16GRNT310200 to FD).

## References

1. Iadecola C. The pathobiology of vascular dementia. Neuron. 2013; 80:844–866. [PubMed: 24267647]
2. Quaegebeur A, Lange C, Carmeliet P. The neurovascular link in health and disease: Molecular mechanisms and therapeutic implications. Neuron. 2011; 71:406–424. [PubMed: 21835339]
3. Zlokovic BV. The blood-brain barrier in health and chronic neurodegenerative disorders. Neuron. 2008; 57:178–201. [PubMed: 18215617]
4. Greenberg SM, Vernooij MW, Cordonnier C, et al. Cerebral microbleeds: A guide to detection and interpretation. Lancet Neurol. 2009; 8:165–174. [PubMed: 19161908]
5. Viswanathan A, Rocca WA, Tzourio C. Vascular risk factors and dementia: How to move forward? Neurology. 2009; 72:368–374. [PubMed: 19171835]
6. Jackson K, Barisone GA, Diaz E, et al. Amylin deposition in the brain: A second amyloid in Alzheimer disease? Ann Neurol. 2013; 74:517–526. [PubMed: 23794448]
7. Oskarsson ME, Paulsson JF, Schultz SW, et al. In vivo seeding and cross-seeding of localized amyloidosis: A molecular link between type 2 diabetes and Alzheimer disease. Am J Pathol. 2015; 185:834–846. [PubMed: 25700985]
8. Schultz N, Byman E, Fex M, et al. Amylin alters human brain pericyte viability and NG2 expression. J Cereb Blood Flow Metab. 2016
9. Westermark P, Andersson A, Westermark GT. Islet amyloid polypeptide, islet amyloid, and diabetes mellitus. Physiol Rev. 2011; 91:795–826. [PubMed: 21742788]
10. Banks WA, Kastin AJ. Differential permeability of the blood-brain barrier to two pancreatic peptides: Insulin and amylin. Peptides. 1998; 19:883–889. [PubMed: 9663454]
11. Beaumont K, Kenney MA, Young AA, et al. High affinity amylin binding sites in rat brain. Mol Pharmacol. 1993; 44:493–497. [PubMed: 8396712]

12. Potes CS, Lutz TA, Riediger T. Identification of central projections from amylin-activated neurons to the lateral hypothalamus. Brain Res. 2010; 1334:31–44. [PubMed: 20382134]
13. Baldo BA, Kelley AE. Amylin infusion into rat nucleus accumbens potently depresses motor activity and ingestive behavior. Am J Physiol Regul Integr Comp Physiol. 2001; 281:R1232–1242. [PubMed: 11557632]
14. Lutz TA. Control of energy homeostasis by amylin. Cell Mol Life Sci. 2012; 69:1947–1965. [PubMed: 22193913]
15. Jurgens CA, Toukatly MN, Fligner CL, et al. Beta-cell loss and beta-cell apoptosis in human type 2 diabetes are related to islet amyloid deposition. Am J Pathol. 2011; 178:2632–2640. [PubMed: 21641386]
16. Huang CJ, Haataja L, Gurlo T, et al. Induction of endoplasmic reticulum stress-induced beta-cell apoptosis and accumulation of polyubiquitinated proteins by human islet amyloid polypeptide. Am J Physiol Endocrinol Metab. 2007; 293:E1656–1662. [PubMed: 17911343]
17. Despa S, Margulies KB, Chen L, et al. Hyperamylinemia contributes to cardiac dysfunction in obesity and diabetes: A study in humans and rats. Circ Res. 2012; 110:598–608. [PubMed: 22275486]
18. Liu M, Verma N, Peng X, et al. Hyperamylinemia increases IL-1beta synthesis in the heart via peroxidative sarcolemmal injury. Diabetes. 2016; 65:2772–2783. [PubMed: 27335231]
19. Gong W, Liu ZH, Zeng CH, et al. Amylin deposition in the kidney of patients with diabetic nephropathy. Kidney Int. 2007; 72:213–218. [PubMed: 17495860]
20. Rebeck GW, Reiter JS, Strickland DK, et al. Apolipoprotein E in sporadic Alzheimer's disease: Allelic variation and receptor interactions. Neuron. 1993; 11:575–580. [PubMed: 8398148]
21. Schmechel DE, Saunders AM, Strittmatter WJ, et al. Increased amyloid beta-peptide deposition in cerebral cortex as a consequence of apolipoprotein E genotype in late-onset Alzheimer disease. Proc Natl Acad Sci U S A. 1993; 90:9649–9653. [PubMed: 8415756]
22. Lei P, Wu WH, Li RW, et al. Prevention and promotion effects of apolipoprotein E4 on amylin aggregation. Biochem Biophys Res Commun. 2008; 368:414–418. [PubMed: 18243137]
23. Charge SB, Esiri MM, Bethune CA, et al. Apolipoprotein E is associated with islet amyloid and other amyloidoses: Implications for Alzheimer's disease. J Pathol. 1996; 179:443–447. [PubMed: 8869295]
24. Guan J, Zhao HL, Sui Y, et al. Histopathological correlations of islet amyloidosis with apolipoprotein E polymorphisms in type 2 diabetic Chinese patients. Pancreas. 2013; 42:1129–1137. [PubMed: 24005233]
25. Westermark P, Engstrom U, Johnson KH, et al. Islet amyloid polypeptide: Pinpointing amino acid residues linked to amyloid fibril formation. Proc Natl Acad Sci U S A. 1990; 87:5036–5040. [PubMed: 2195544]
26. Couce M, Kane LA, O'Brien TD, et al. Treatment with growth hormone and dexamethasone in mice transgenic for human islet amyloid polypeptide causes islet amyloidosis and beta-cell dysfunction. Diabetes. 1996; 45:1094–1101. [PubMed: 8690157]
27. Matveyenko AV, Butler PC. Islet amyloid polypeptide (IAPP) transgenic rodents as models for type 2 diabetes. ILAR J. 2006; 47:225–233. [PubMed: 16804197]
28. Srodulski S, Sharma S, Bachstetter AB, et al. Neuroinflammation and neurologic deficits in diabetes linked to brain accumulation of amylin. Mol Neurodegener. 2014; 9:30. [PubMed: 25149184]
29. Verma N, Ly H, Liu M, et al. Intraneuronal amylin deposition, peroxidative membrane injury and increased IL-1beta synthesis in brains of Alzheimer's disease patients with type-2 diabetes and in diabetic HIP rats. J Alzheimers Dis. 2016; 53:259–272. [PubMed: 27163815]
30. Ilaiwy A, Liu M, Parry TS, et al. Human amylin proteotoxicity impairs protein biosynthesis, and alters major cellular signaling pathways in the heart, brain and liver of humanized diabetic rat model in vivo. The FASEB Journal. 2016; 30:lb461.
31. Moreno-Gonzalez I, Edwards G Iii, Salvadores N, et al. Molecular interaction between type 2 diabetes and Alzheimer's disease through cross-seeding of protein misfolding. Mol Psychiatry. 2017

32. Biessels GJ, Staekenborg S, Brunner E, et al. Risk of dementia in diabetes mellitus: A systematic review. Lancet Neurol. 2006; 5:64–74. [PubMed: 16361024]
33. Luitse MJ, Biessels GJ, Rutten GE, et al. Diabetes, hyperglycaemia, and acute ischaemic stroke. Lancet Neurol. 2012; 11:261–271. [PubMed: 22341034]
34. Ott A, Stolk RP, van Harskamp F, et al. Diabetes mellitus and the risk of dementia: The Rotterdam study. Neurology. 1999; 53:1937–1942. [PubMed: 10599761]
35. Ismail-Beigi F, Craven T, Banerji MA, et al. Effect of intensive treatment of hyperglycaemia on microvascular outcomes in type 2 diabetes: An analysis of the ACCORD randomised trial. Lancet. 2010; 376:419–430. [PubMed: 20594588]
36. Ohara T, Doi Y, Ninomiya T, et al. Glucose tolerance status and risk of dementia in the community: The Hisayama study. Neurology. 2011; 77:1126–1134. [PubMed: 21931106]
37. Abner EL, Nelson PT, Kryscio RJ, et al. Diabetes is associated with cerebrovascular but not Alzheimer's disease neuropathology. Alzheimers Dement. 2016; 12:882–889. [PubMed: 26812281]
38. Nelson PT, Smith CD, Abner EA, et al. Human cerebral neuropathology of Type 2 diabetes mellitus. Biochimica et biophysica acta. 2009; 1792:454–469. [PubMed: 18789386]
39. Mirra SS, Heyman A, McKeel D, et al. The consortium to establish a registry for Alzheimer's disease (CERAD). Part II. Standardization of the neuropathologic assessment of Alzheimer's disease. Neurology. 1991; 41:479–486. [PubMed: 2011243]
40. Braak H, Braak E. Neuropathological stageing of Alzheimer-related changes. Acta neuropathologica. 1991; 82:239–259. [PubMed: 1759558]
41. Nelson PT, Jicha GA, Schmitt FA, et al. Clinicopathologic correlations in a large Alzheimer disease center autopsy cohort: Neuritic plaques and neurofibrillary tangles "do count" when staging disease severity. Journal of neuropathology and experimental neurology. 2007; 66:1136–1146. [PubMed: 18090922]
42. Schmitt FA, Nelson PT, Abner E, et al. University of Kentucky Sanders-Brown healthy brain aging volunteers: donor characteristics, procedures and neuropathology. Current Alzheimer research. 2012; 9:724–733. [PubMed: 22471862]
43. Nelson PT, Pious NM, Jicha GA, et al. Apoe-ε2 and Apoe-ε4 correlate with increased amyloid accumulation in cerebral vasculature. Journal of neuropathology and experimental neurology. 2013; 72:708–715. [PubMed: 23771217]
44. Hu R, Zhang M, Patel K, et al. Cross-sequence interactions between human and rat islet amyloid polypeptides. Langmuir. 2014; 30:5193–5201. [PubMed: 24754490]
45. Sander JD, Joung JK. CRISPR-Cas systems for editing, regulating and targeting genomes. Nat Biotechnol. 2014; 32:347–355. [PubMed: 24584096]
46. Vorhees CV, Williams MT. Morris water maze: Procedures for assessing spatial and related forms of learning and memory. Nat Protoc. 2006; 1:848–858. [PubMed: 17406317]
47. Okubo S, Strahle J, Keep RF, et al. Subarachnoid hemorrhage-induced hydrocephalus in rats. Stroke. 2013; 44:547–550. [PubMed: 23212164]
48. Shim YS, Yang DW, Roe CM, et al. Pathological correlates of white matter hyperintensities on magnetic resonance imaging. Dement Geriatr Cogn Disord. 2015; 39:92–104. [PubMed: 25401390]
49. Despa S, Sharma S, Harris TR, et al. Cardioprotection by controlling hyperamylinemia in a "humanized" diabetic rat model. J Am Heart Assoc. 2014; 3(4):e001015. [PubMed: 25146704]
50. Pantoni L. Cerebral small vessel disease: From pathogenesis and clinical characteristics to therapeutic challenges. Lancet Neurol. 2010; 9:689–701. [PubMed: 20610345]
51. Hainsworth AH, Markus HS. Do in vivo experimental models reflect human cerebral small vessel disease? A systematic review. J Cereb Blood Flow Metab. 2008; 28:1877–1891. [PubMed: 18698331]
52. Sozmen EG, Hinman JD, Carmichael ST. Models that matter: White matter stroke models. Neurotherapeutics. 2012; 9:349–358. [PubMed: 22362423]
53. Mahley RW. Apolipoprotein E: Cholesterol transport protein with expanding role in cell biology. Science. 1988; 240:622–630. [PubMed: 3283935]

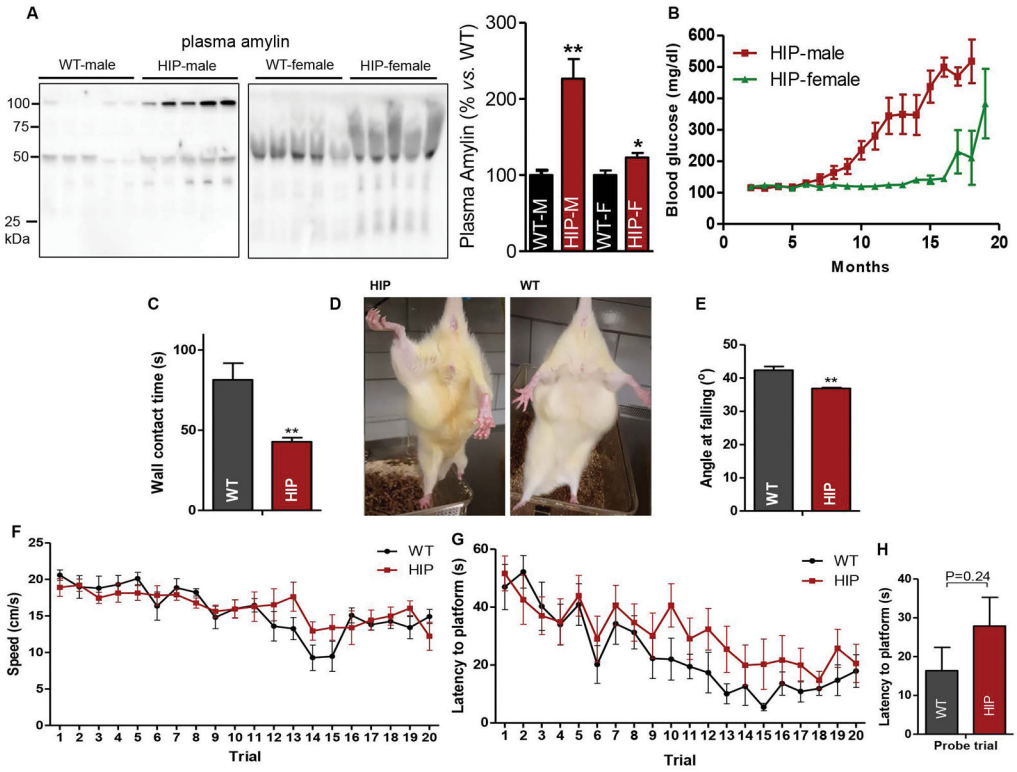


**Fig. 1.**

Amylin, blood glucose and neurologic deficits in HIP rats. A. Western blot analysis of amylin in plasma from HIP and wild type (WT) male and female littermates, 15 months of age (M-male, F-female). B. Blood glucose in HIP and WT male and female littermates. C. Spontaneous forelimb use in male HIP rats vs. WT littermates assessed at 15 months of age by forepaws-to-wall contact time during vertical rearing up in the cylinder test (n = 5). D. Pathologic hind limb clasping in a 15 months old male HIP rat compared to a WT littermate rat. E. Inclined plane test in 15 months old male HIP rats vs. WT rat littermates (n = 5). F. Swim speed for HIP and WT rats in the Morris water maze test (n = 10, 15–16 months old). G. Latency for HIP and WT rats to swim to target platform in Morris water maze test (n = 10, 15–16 months old rats). H. Latency to platform in the probe trial. Error bars represent mean ± SEM; $^{**}P < 0.01$; $^{***}P < 0.0001$; by unpaired two-tailed Student's *t* test (E,G,H–J), log-rank test (B,C).

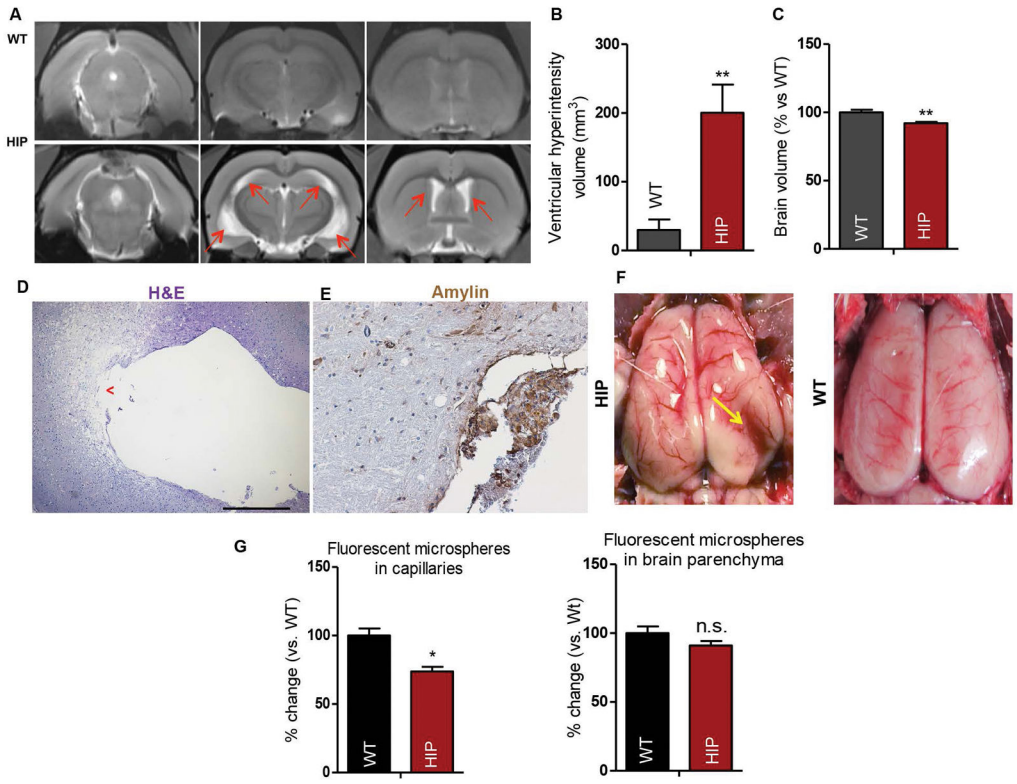


**Fig. 2.**

Periventricular injury and hypoperfusion in HIP rats. A. Three slices (1, 3 and 5 out of 7 consecutive slices 1mm apart) of coronal $T_2$-weighted MR images comparing the brains of a 15 months old male HIP rat vs. a WT littermate rat. Hyperintensity areas (↑) in the lateral hippocampus and temporal horns of HIP rats reflect extracellular fluid accumulation. B,C. Volumes of ventricles and brain parenchyma in male HIP and WT littermate rats computed from coronal $T_2$-weighted MR images; 1 image pixel area = 0.024 $mm^2$ (n = 7). D. Hematoxylin and Eosin (H&E) staining of the lateral ventricle area in brains of HIP rats with considerably enlarged ventricles. E. Immunohistochemistry analysis with an amylin antibody of the choroid plexus in the same rat as in (D). F. Example of intracerebral hemorrhages (↑) that occured in male HIP rats, but not WT littermates (>12 months of age). G. Cerebral perfusion in male HIP and WT rats at ~15 months of age (n = 3) assessed by the retrieval from brain capillaries and parenchyma of intravenously infused fluorescent microspheres. Experiments were repeated three times for all representative images. Error bars represent mean ± SEM; *$P < 0.05$; **$P < 0.01$; n.s., not significant; by unpaired two-tailed Student's *t* test (B,C,F). Scale bar, 500 μm in D and 100 μm in E.

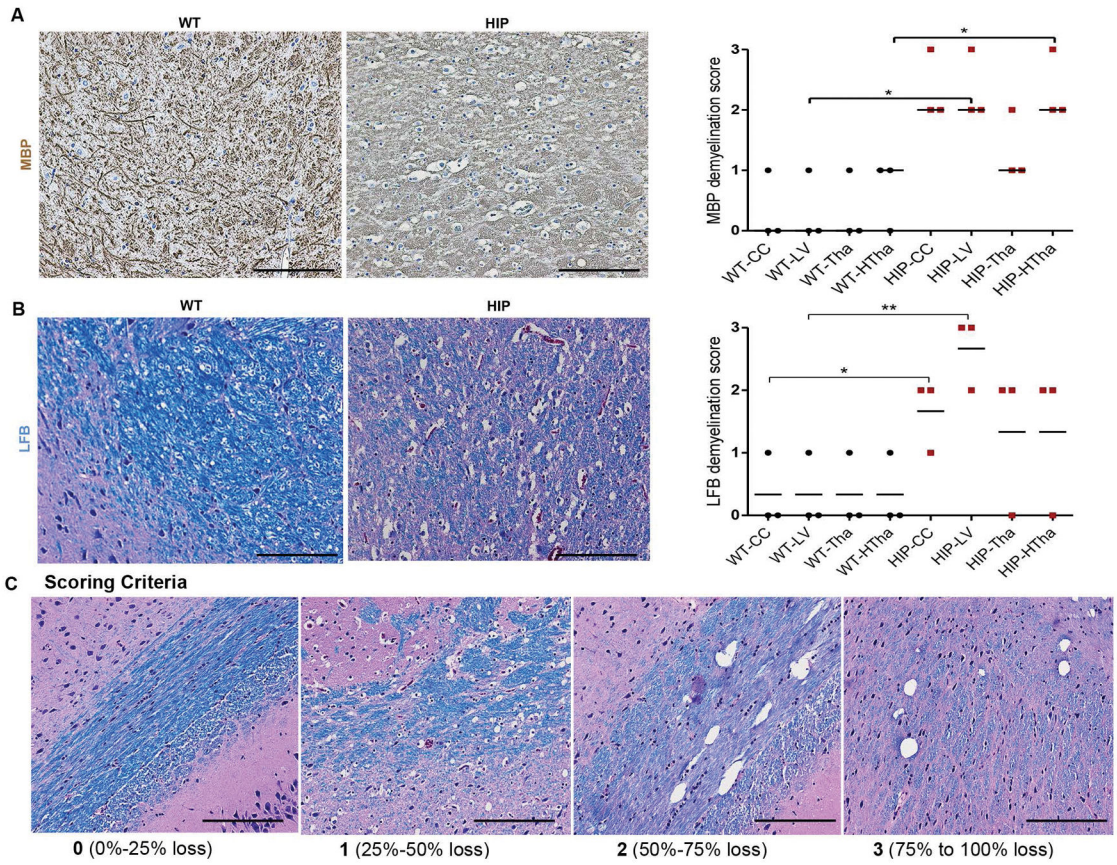


**Fig. 3.**

White matter rarefaction in HIP rats. A. Representative immunohistochemical (IHC) analysis of myelin basic protein (MBP) in the hypothalamus (htha) of a 15 months old male HIP rat vs. a WT littermate rat. Analysis (graph) of MBP level in HIP and WT brain white matter areas (cc- corpus callosum; lv- lateral ventricle area; tha- thalamus; htha- hypothalamus) (n = 3). B. Representative IHC analysis of myelin level assessed by Luxol fast blue (LFB) staining in the hypothalamus (htha) of a 15 months old male HIP rat vs. a WT littermate rat. Analysis was carried out in the same brain areas as in above (n = 3). C. Scoring criteria for demyelination in myelin binding protein and Luxol fast blue staining. Exampled images of Luxol fast blue staining of HIP rat brain tissues. Experiments were repeated three times for all representative images. Error bars represent mean ± SEM; $*P < 0.05$; $**P < 0.01$; n.s., not significant; by Mann-Whitney unpaired two-tailed *t* test. Scale bar, 100 μm.

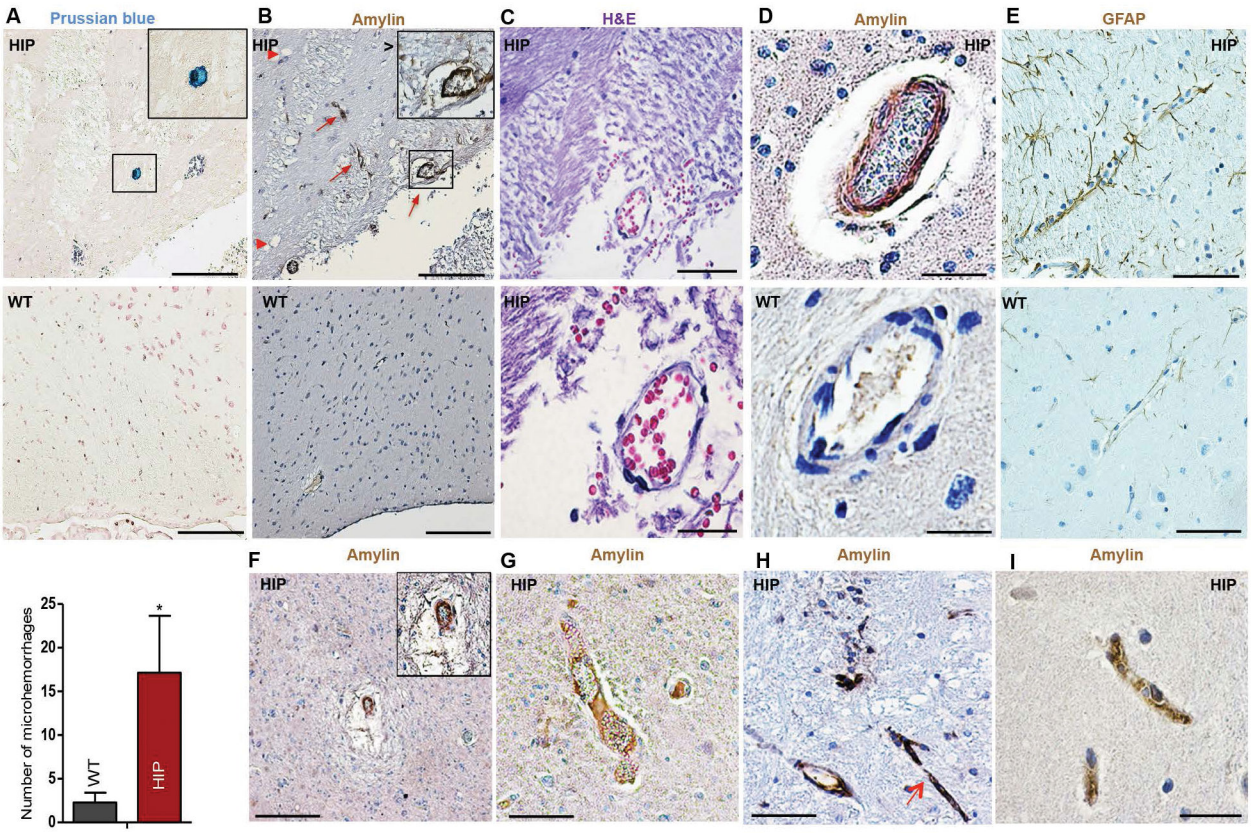


**Fig. 4.**

Brain microhemorrhages and perivascular astrocyte recruitment in HIP rats.

A. Analysis of the number of brain microhemorrhages stained with Prussian blue dye in HIP vs. WT rats (n = 7). Representative staining with Prussian blue dye of a microhemorrhage in the lateral hypothalamus-ventricular area of a 15 months old HIP rat. Same brain area from a WT rat is the control. B. Representative image of serial staining with an amylin antibody in the same brain region as in (A) shows amylin deposits in microvessels (↑) and perivascular area (inset; brown deposits) in HIP rats but not WT rats. White matter vacuolation (▲) was found in HIP rat brains. C. Images with a higher magnification (40× and 100×, respectively) of the same brain area stained with H&E D. Representative IHC analysis of amylin in a small arteriole (HIP vs. WT rats). E. Representative IHC analysis of activated astrocytes in areas of vascular injury in the brain of a HIP rat assessed by staining for glial fibrillary acidic protein (GFAP, brown). Images are from hypothalamus. Same area from a WT rat brain is the control. F–H. IHC analysis of amylin in areas of microvascular injury in HIP rat brains. I. Representative IHC analysis of vascular amylin deposition in the hippocampus of a HIP rat. Error bars represent mean ± SEM; $*P < 0.05$; by unpaired two-tailed Student's $t$ test (A). Experiments are repeated three times for all representative images. Scale bar, 100 μm in A,B,F; 50 μm in C (top) E,G,H; 20 μm in D and 10 μm in C (lower panel) and I.

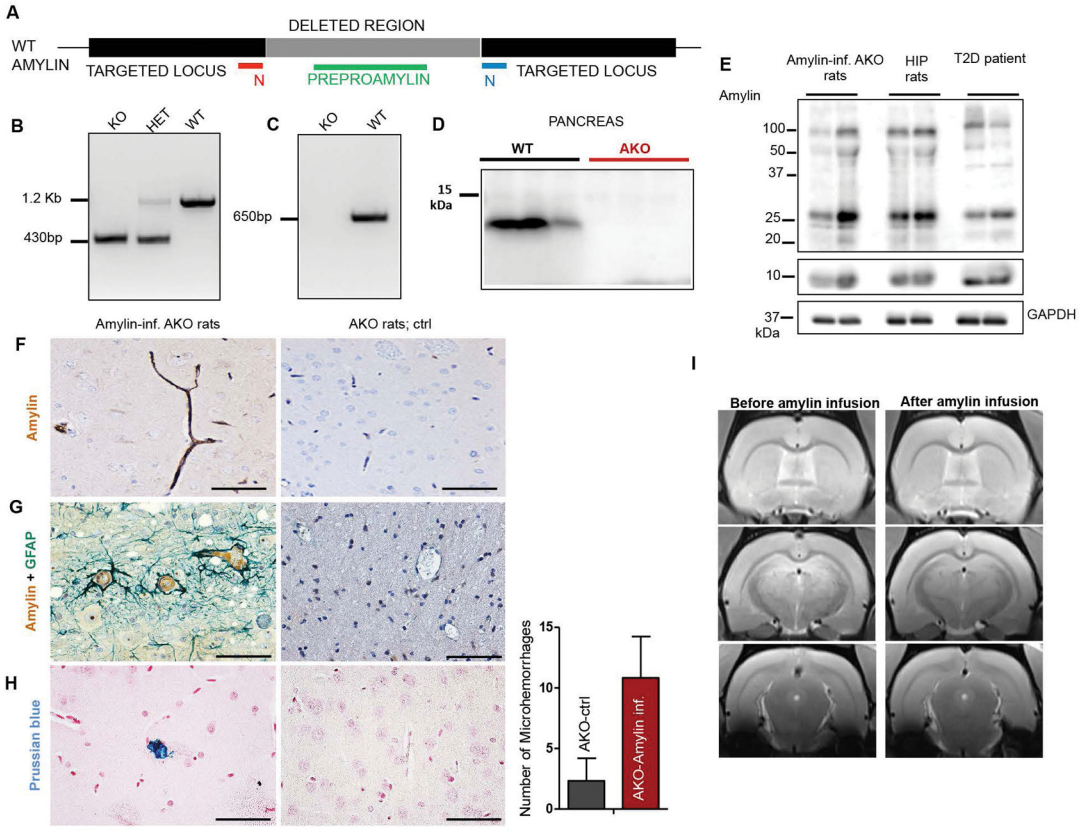


**Fig. 5.**

Infusion of aggregated amylin in amylin knockout (AKO) rats. A. Amylin gene deletion with CRISPR/CAS9. The two cut guide sites are shown below in bold. Preproamylin nucleotide sequence is shown in green. Deleted region:

“agagctaagcaagttgagggatatataagagtcagctcgccgattaccaagccgtgcgtgcacgcttgggctgtagttcctgaagct tcaggctgccagcacactatctgttattgctgccactgcccactg**N**aaaggtaaaggatcccccgtgctttggaagatattacttagta aaagaaaaccgtctttgtgttacccgtaggacacatttcaggaaaaagagtaaatgaatagtgtgttatagtaaaaattctcaggctgttt ttaaaagaaaattgaacatttggaactatttcaaagatgataagcatcagagatctctttgtaaaataaacttaaatttccttgatggttcc aatttacacttgtgtcaaccagaactgaaggaggtggtttgacttcggtgttctttcttttcagggatcttgagacatgaggtgcatctcca ggctgccagctgttctcctcatcctctcggtggcactcggccacttgagagctacacctgtcggaaggttggtgacctgaacattccta cctcctttgaaaagtgtggggaaatcaggattccacagtgctatgtaatgaataccctctgtgttgtttaatttctacgtaaatactggcaa cgagaagtacttggggctgaatggtttcataaccctgtgttctttaaggacaaggtcagcagctgaggattggctcgtaggacgtttagt agaaggcatcattagagacgtttgcctgaaaatggtttagaacctacaggggtaaagctagggtagactaacagggcaactgagaca cagacattcaccctgttgaatgcagtactgaaagaaactgaaggaatgccaaccaaaaataaaatgttttcatgtcaattggaatcttga tgaatacttataggttcttttccctgctcaggggNgatctgtaagtatccaaacttctacatcttcttctgaaaaccgacgtcataaaaata ggaagtggggttggggatttagctcagtggtagagcacttgcccagcaagtgcaaagccctgggttcggtccccagctccggaaaa aaaaataggaagcaaatgcatggctttaaggagttaaatttaggattagttttaaagtcatctgaaagtcattccatacatgacattacag agatataagaagttattctgcatcagaaggtgacttctgggcctctgtgaatgtgaactagtgg”

B. Gel electrophoresis showing a ~ 1.2 kb from the WT rat amylin DNA and a ~ 430 bp sequence remaining after deletion of amylin gene. C. Gel electrophoresis showing a 650 bp sequence that includes part of the amylin gene that was deleted in transgenic animals. D.

Western blot analysis of pancreatic tissues demonstrating that the protein level of amylin is reduced in the AKO rats compared to WT littermates. E. Cropped Western blot of amylin in blood lysates from amylin-infused AKO rats, HIP rats and type-2 diabetes (T2D) patients. Amylin band at ~10 kDa (the amylin dimer) required longer exposure time and is displayed separately. Experiments are repeated twice. F,G. Representative images of IHC staining with amylin (F) and co-staining for amylin (brown) and GFAP (green) (G) in the cerebral cortex of an amylin-infused AKO rat vs. an age-matched AKO rat without amylin infusion (n = 3). H. Prussian blue dye in the brain cortex area of an amylin-infused AKO rat vs. an age-matched AKO rat without amylin infusion. Analysis of the number of brain microhemorrhages in amylin-infused AKO and control AKO rats (n = 6). I. Three slices (1, 3 and 5 out of 7 consecutive slices 1mm apart) of coronal $T_2$-weighted MR images comparing the brain in an AKO rat before and after infusion with aggregated human amylin (2 μg/g body weight, q.d., 7 days) (n = 3).

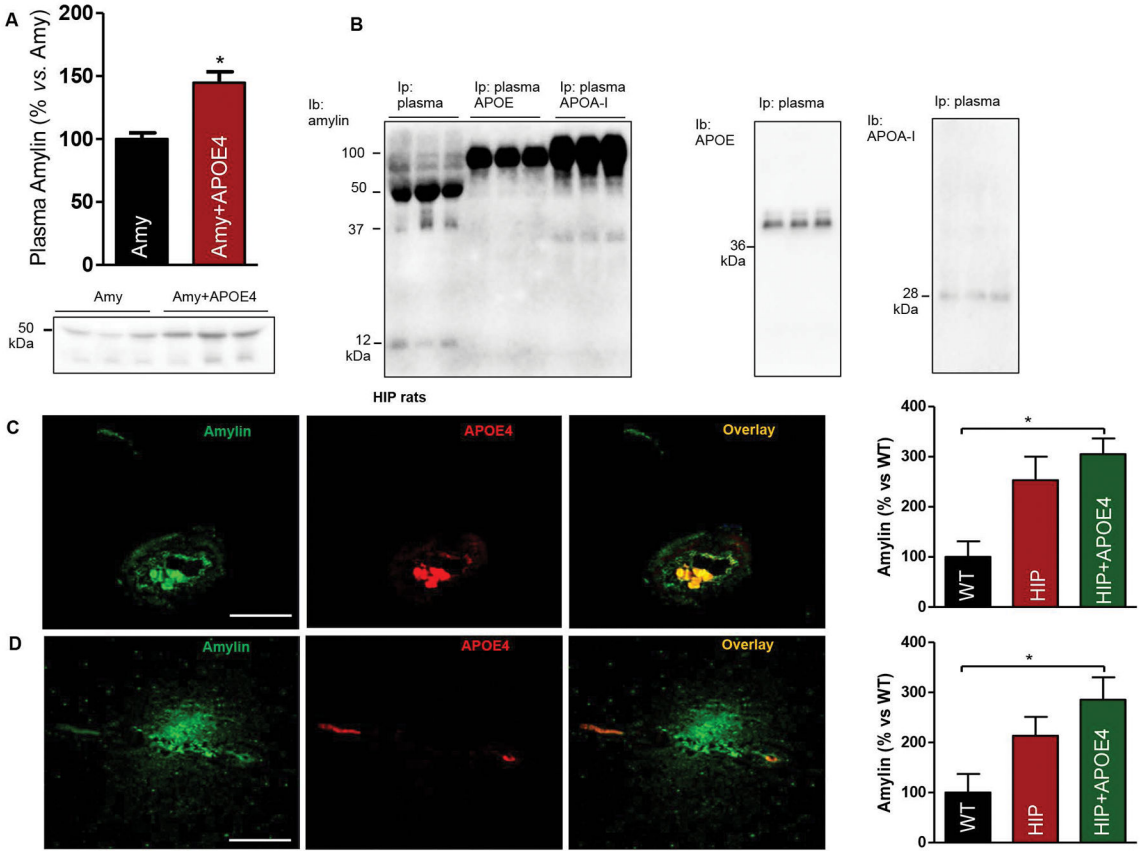


**Fig. 6.**

Amylin interaction with plasma apolipoproteins *in vivo*. A. Cropped Western blot of amylin in plasma from AKO rats infused with amylin alone or in combination with APOE4 (n = 3). B. Western blot analysis with an anti-amylin antibody of HIP rat plasma samples that were enriched in APOE or APOA-1 by immunoprecipitation. (n = 3). C. Representative immunofluorescence images of amylin-APOE4 vascular deposition in brain microvessels of HIP rats injected with human APOE4. Analysis of amylin fluorescence intensity in the brain blood vessels of WT, HIP and APOE4-infused HIP rats (graph; n = 3). D. Same as in C for brain parenchyma. The bar graph shows analysis of amylin fluorescence intensity in brain parenchyma of WT, HIP and APOE4-infused HIP rats (n = 3). Error bars represent mean ± SEM; $*P < 0.05$. $**P < 0.01$, $***P < 0.0001$; by unpaired two-tailed Student's *t* test. Scale bars, 50 μm in B–D; 20 μm in G and H.

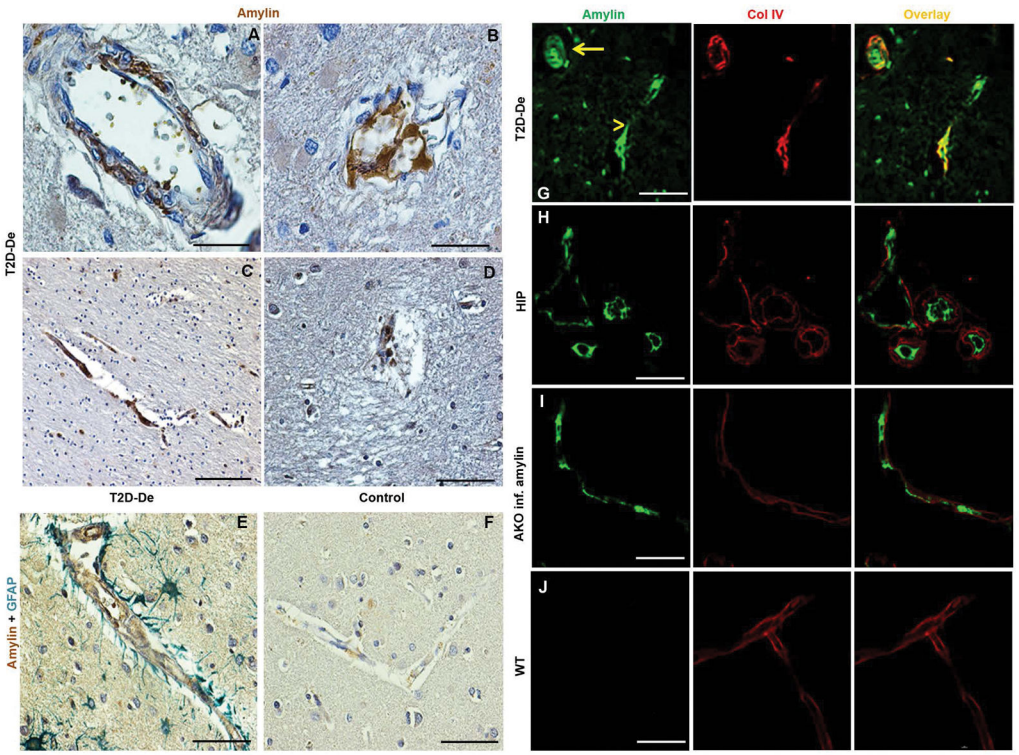


**Fig. 7.**

Cerebral amylin vasculopathy in patients with dementia and type-2 diabetes (T2D-De), HIP rats and amylin-infused AKO rats. A–D. Representative IHC analysis of amylin deposition (brown) in the brain blood vessels of T2D-De patients (n = 3 patients). E. Representative IHC showing co-staining of GFAP (green) and amylin (brown) in areas of cerebral vascular injury on brain sections from the same T2D-De patients as in A–D. F. Representative IHC analysis with amylin and GFAP antibodies on brain sections from healthy aged individuals (Ctl; n = 3). G. Representative immunofluorescence images of amylin deposition (green) on the luminal side of the vessel basement membrane stained with Collagen IV (red) in the brain microvessels of T2D-De patients (n = 3). H–J. Representative immunofluorescence images of amylin deposition (green) on the luminal side of vessel basement membrane stained with Collagen IV (red) in the brain microvessels of HIP rats (H; n = 3), amylin-infused AKO rats (i; n = 3) and age-matched WT rat brains (J; n = 3). Experiments are repeated twice for all representative images. Scale bars, 10 μm in A,B; 20 μm in G–J; 50 μm in D–F and 100 μm in C.

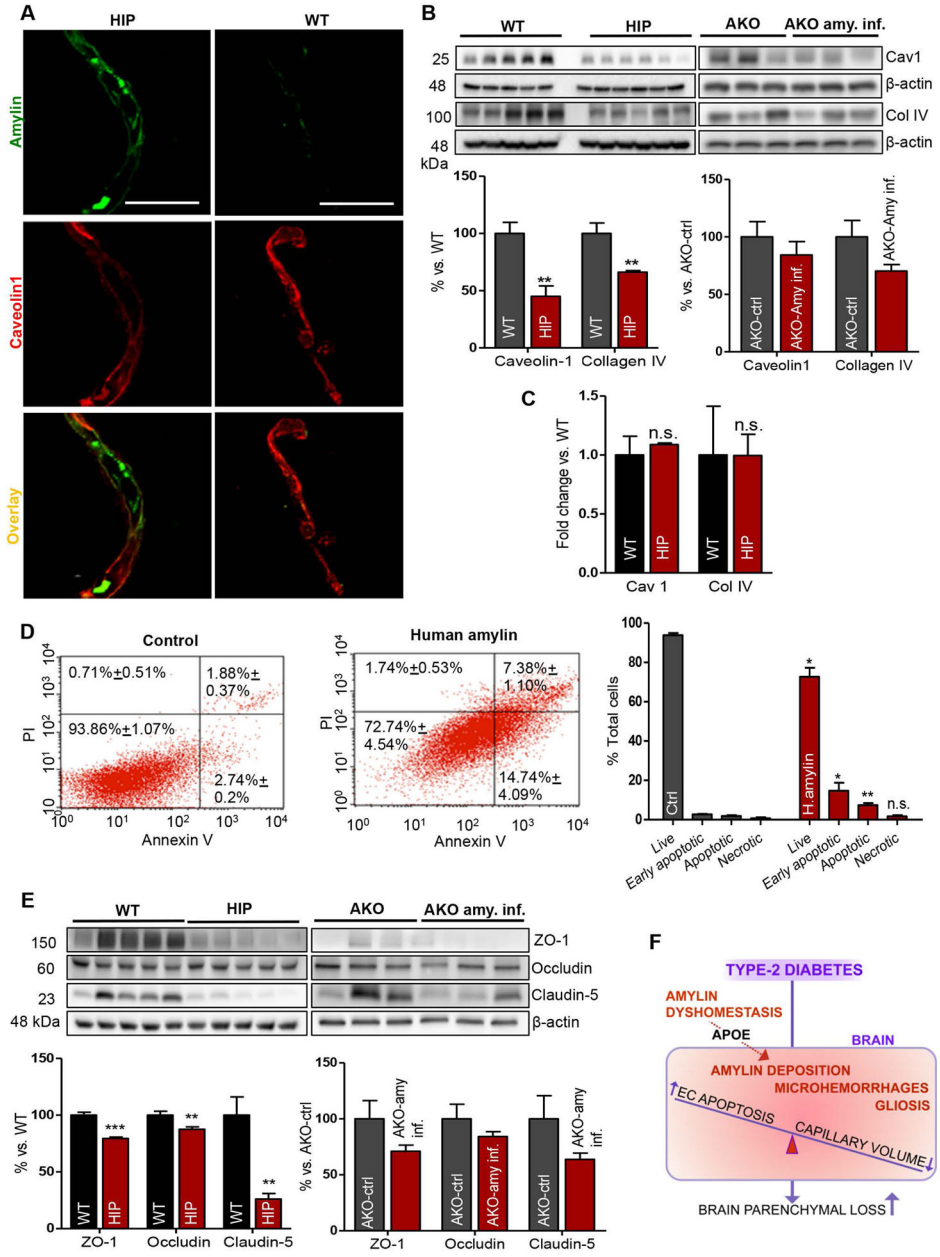


**Fig. 8.**

Vascular amylin deposition injures endothelial cells and degrades tight junction components. A. Representative immunofluorescence images of isolated brain capillaries from HIP and WT littermate rats (15 months old) showing endothelial cells (caveolin1, red) and amylin deposition (green) (n = 3 rats). Scale bar, 10 μm. Experiments are repeated twice for all representative images and results. B. Cropped Western blot of caveolin-1 (Cav1) and collagen IV (Col IV) in capillary lysates from HIP and WT rats (n = 5; left panel), and amylin-infused AKO and control AKO (no amylin) rats (n = 3; right panel). Corresponding densitometry analyses of caveolin1 and collagen IV levels are displayed in the lower panel. C. Quantitative real-time PCR of caveolin1 and collagen IV mRNA in isolated capillaries

from HIP and WT rats (caveolin1, n = 4; collagen IV, n = 3). D. Flow cytometry analysis of rat brain microvascular endothelial cells apoptosis when incubated with 50 μM human amylin (n = 3). Apoptotic cells are detected with Annexin V (AnV) and dead cells are detected with Propidium Iodide (PI). Live cells are AnV−/PI−, early apoptotic cells are AnV +/PI−, end-stage apoptotic cells are AnV+/PI+, necrotic cells are AnV−/PI+. E. Cropped Western blot of endothelial cell tight junction proteins (ZO-1, occludin, and claudin-5) in capillary lysates from HIP and WT brain (n = 5; left panel), and amylin-infused AKO and control AKO rats (n = 3; right panel). F. Proposed mechanism: aggregated amylin causes endothelial dysfunction and microvascular injury and is modulated by amylin transport in the brain via plasma APOE. Corresponding densitometry analyses of tight junction protein levels are displayed in the lower panel. Error bars represent mean ± SEM; $*P < 0.05$, $**P < 0.01$, $***P < 0.001$, n.s., not significant; by unpaired two-tailed Student's *t* test (B,C,D,E,F,G).